DOI: 10.1002/ejic.201001037

Favorable Protonation of the (μ-edt)[$Fe_2(PMe_3)_4(CO)_2$(H-terminal)]$^+$ Hydrogenase Model Complex Over Its Bridging μ-H Counterpart: A Spectroscopic and DFT Study

Mary Grace I. Galinato,[a] C. Matthew Whaley,[b] Dean Roberts,[c] Peng Wang,[c] and Nicolai Lehnert*[a]

Keywords: [FeFe] hydrogenases / Protonation / Enzyme models / Density functional calculations / Raman spectroscopy / IR spectroscopy / Potential energy surface / Electronic structure

The mechanism of hydrogen production in [FeFe] hydrogenase remains elusive. However, a species featuring a terminal hydride bound to the distal Fe is thought to be the key intermediate leading to hydrogen production. In this study, density functional theory (DFT) calculations on the terminal (*H*-term) and bridging (μ-H) hydride isomers of (μ-edt)-[$Fe_2(PMe_3)_4(CO)_2H$]$^+$ are presented in order to understand the factors affecting their propensity for protonation. Relative to *H*-term, μ-H is 12.7 kcal/mol more stable, which contributes to its decreased reactivity towards an acid. Potential energy surface (PES) calculations for the reaction of the *H*-term isomer with 4-nitropyridinium, a proton source, further reveal a lower activation energy barrier (14.5 kcal/mol) for *H*-term than for μ-H (29 kcal/mol). Besides these energetic considerations, the *H*-term isomer displays a key molecular orbital (MO <139>) that has a relatively strong hydride (1s) contribution (23 %), which is not present in the μ-H isomer. This indicates a potential orbital control of the reaction of the hydride complexes with acid. The lower activation energy barrier and this key MO together control the overall catalytic activity of (μ-edt)[$Fe_2(PMe_3)_4(CO)_2$(H-term)]$^+$. Lastly, Raman and IR spectroscopy were performed in order to probe the ν(Fe-H) stretching mode of the two isomers and their deuterated counterparts. A ν(Fe-H) stretching mode was observed for the μ-H complex at 1220 cm^{-1}. However, the corresponding mode is not observed for the less stable *H*-term isomer.

Introduction

Hydrogen is particularly interesting as an alternative energy carrier because its combustion is clean and only produces water. In addition, hydrogen has an unmatched energy density and is therefore a desirable fuel. In nature, two types of enzymes containing Fe or Ni dimetallic centers exist that either produce or oxidize H_2; these are the [FeFe][1,2] and [NiFe][3,4] hydrogenases, respectively. A third type of hydrogenase that has no sequence similarity to either the [FeFe] or the [NiFe] enzyme is the H_2-forming methylene-tetrahydromethanopterin dehydrogenase (or Hmd), which unlike the dimetallic hydrogenases only contains a mononuclear non-heme iron center.[5,6] Among these different enzymes, the [FeFe] hydrogenase is known to be the most efficient catalyst, producing 6000–9000 molecules of H_2/s per enzyme molecule at 30 °C,[7] which is 10–100 times more active than its [NiFe] counterpart.[8] In addition, the active site is very stable and only contains the inexpensive metal iron, which establishes its potential as an economical H_2-forming catalyst. For these reasons, we focus on the active site of the [FeFe] hydrogenase to better understand the enzyme's ability to catalyze hydrogen production with high efficiency.

The catalytic site of [FeFe] hydrogenase consists of an Fe–Fe center bridged by a bis(thiomethyl)amine ligand and CN^- and CO ligands attached to the diiron center (Scheme 1).[9–13] This unique structure has prompted the design of many synthetic mimics, some of which model proposed intermediates in the catalytic cycle of the enzyme, and actually produce hydrogen.[14–50] Two possible structures of the key protonated intermediate of [FeFe] hydrogenase have been identified by using model complexes: the first has a semi-bridging CO ligand and a hydride terminally bound (*H*-term) to the distal iron, Fe_d (Scheme 1), while the second has two terminal CO ligands and a hydride bridging (μ-H) the distal and proximal (Fe_p) iron centers. Electronic absorption spectroscopy/DFT studies on an Fe^I–Fe^I model complex imply that the shift of the μ-CO group towards the distal Fe atom should increase the nucleophilic character of this Fe site,[51] which then favors protonation at this iron center instead of the Fe–Fe bond and generates *H*-term.[51,52] In contrast, the hypothesis of μ-H formation

[a] Department of Chemistry, University of Michigan, Ann Arbor, MI 48109, USA
Fax: +1-734-615-3790
E-mail: lehnertn@umich.edu
[b] Department of Chemistry, University of Illinois at Urbana-Champaign, Urbana, IL 61801, USA
[c] Bruker Optics Inc. 19 Fortune Drive, Manning Park, Billerica, MA 01821, USA
Supporting information for this article is available on the WWW under http://dx.doi.org/10.1002/ejic.201001037.

as an intermediate is supported by the low energy barrier for heterolytic cleavage of H_2 (4.5–6.2 kcal/mol),[53] considering the back reaction, and the high stability of μ-H as demonstrated by model complexes[16,21,54–56] and DFT calculations.[53,57,58] A recent study on a series of [FeFe] hydrogenase model complexes shows the formation of a μ-H species, and not *H*-term, upon protonation.[59,60] The structures of the two intermediates have also been proposed on the basis of two opposing ideas with respect to the binding site of H_2, whether it is at the distal (*H*-term) or proximal (μ-H) iron center. Proponents supporting the *H*-term intermediate suggest that binding of H_2 to the distal iron atom increases its acidity, favors heterolytic cleavage, and results in *H*-term formation.[61–65] It has also been suggested that the role of the bridging CO (μ-CO) is to prevent μ-H formation by steric effects.[51,52]

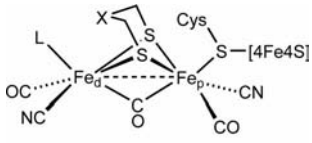

X = CH_2 (pdt), NH (dta), or O (dte)
L = vacant, H, H_2, CO, or H_2O

Scheme 1. H cluster of [FeFe] hydrogenase.

One key result in this respect is the observation that the less-stable *H*-term isomer of (μ-edt)[$Fe_2(PMe_3)_4(CO)_2H$]$^+$ (Figure 1) produces H_2 upon reaction with acid,[66] whereas the corresponding μ-H complex is unreactive under these conditions. The ability of this mimic to catalyze the production of H_2 is of high significance, which is the focus of this study. Interestingly, this observation parallels diborane chemistry, where calculations show that the terminal hydride can be protonated but not the bridging hydride.[67] The underlying factor(s) influencing the preferential protonation of *H*-term over μ-H have not been addressed in the literature. In this study, potential energy surfaces (PES) are generated through density functional theory (DFT) calculations for the reactions of the *H*-term and μ-H isomers of (μ-edt)[$Fe_2(PMe_3)_4(CO)_2H$]$^+$ with a proton source in order to determine the activation energy barriers of the proton transfer reaction and the relative stability of the products. Further analysis of the molecular orbital (MO) diagrams allows us to gain additional insight into other factors that potentially affect the reactivity of these complexes towards acids, such as atomic charge and hydride contribution to key MOs. Besides the comparison of calculated and experimental geometries, we further tried to assess the quality of the description of the Fe–H and Fe–CO bonds obtained from DFT using vibrational spectroscopy. Although the optimized geometries of both isomers are in good agreement with the crystal structures, vibrational frequencies would be a better mode of comparison. In particular, Raman and IR spectroscopy were performed in order to identify the Fe–H stretching mode, ν(Fe–H), and the C=O stretching modes, ν(C=O), in the terminal and bridging hydride isomers of (μ-edt)[$Fe_2(PMe_3)_4(CO)_2H$]$^+$. In this respect, note that ν(Fe–H) has never been reported for any [FeFe] hydrogenase model or the enzyme itself. In summary, this study constitutes a detailed theoretical and vibrational investigation of the catalytically active, protonated hydrogenase model complex, (μ-edt)[$Fe_2(PMe_3)_4(CO)_2H$]$^+$. These results provide the necessary groundwork in understanding the spectroscopic and electronic structural differences between the *H*-term and μ-H isomers in detail, and their differing reactivity towards acids.

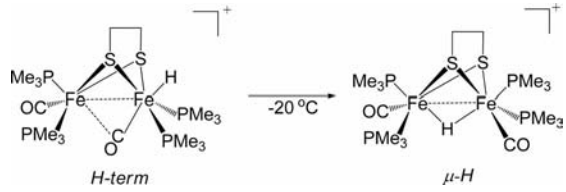

Figure 1. [FeFe] hydrogenase model complex (μ-edt)[$Fe_2(PMe_3)_4(CO)_2H$]$^+$ showing the conversion of the terminal (*H*-term) to the bridging hydride (μ-H) isomer.[66]

Results and Discussion

DFT Geometry Optimizations

The geometry-optimized (BP86/TZVP)[68] structures of the *H*-term and μ-H isomers of (μ-edt)[$Fe_2(PMe_3)_4(CO)_2H$]$^+$ shown in Figure 2 closely resemble the respective crystal structures. For example, *H*-term has a Fe(1)–Fe(2) distance of 2.567 Å in the crystalline form,[66] which is comparable to 2.608 Å in the optimized structure. The Fe(2)–H bond lengths for the crystal and calculated structures are 1.512 Å[66] and 1.530 Å, respectively. The Fe(1)–C(1) and Fe(2)–C(1) distances in the crystal structure (2.443 and 1.771 Å,[66] respectively) are again comparable to the optimized structure (2.517 and 1.782 Å, respectively). For the μ-H complex, the Fe(1)–Fe(2) distance in the crystal is 2.610 Å, which is similar to that of the optimized structure (2.644 Å). The experimental Fe(1)–H and Fe(2)–H distances are 1.653 and 1.612 Å, respectively, which are reproduced well by DFT (1.676 and 1.675 Å, respectively). Table 1 lists selected bond lengths and angles of the experimental and BP86/TZVP optimized structures of the hydride isomers of (μ-edt)[$Fe_2(PMe_3)_4(CO)_2H$]$^+$. The excellent agreement between experiment and calculations observed here is crucial in obtaining a good description of the elec-

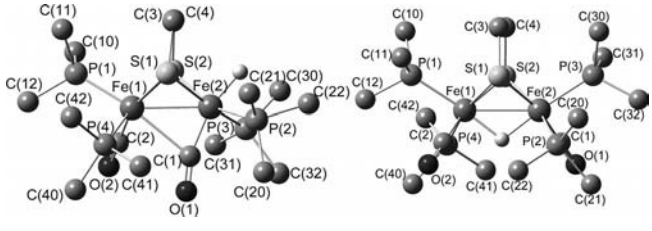

Figure 2. Optimized structures (BP86/TZVP) of the *H*-term (left) and μ-H (right) isomers of (μ-edt)[$Fe_2(PMe_3)_4(CO)_2H$]$^+$, with the atomic labeling scheme. Hydrogen atoms of organic side chains are omitted for clarity.

tronic properties of the two complexes, as will be discussed in the next section. In addition to the overall structure of the optimized complexes, it is noteworthy to compare relative energies of the two isomers. Relative to *H*-term, μ-H is 12.7 kcal/mol more stable. This suggests that the decreased reactivity of μ-H towards acid[66] could be due to the distinctively lower total energy of this complex relative to *H*-term. Other possible factors contributing to its decreased reactivity are presented in the following sections.

Table 1. Selected bond lengths [Å] and angles [°] in (μ-edt)[$Fe_2(PMe_3)_4(CO)_2H]^+$.

	H-term		μ-H	
	X-ray[66]	DFT	X-ray[66]	DFT
Fe(1)–Fe(2)	2.567	2.608	2.610	2.644
Fe(1)–H	–	–	1.653	1.676
Fe(2)–H	1.512	1.530	1.612	1.675
Fe(1)–C(1)	2.443	2.517	1.738	1.746
Fe(2)–C(1)	1.771	1.782	1.754	1.746
Fe(2)–Fe(1)–C(1)	41	41	–	–
Fe(1)–Fe(2)–C(1)	66	67	26	26
Fe(2)–Fe(1)–H	–	–	36	38
Fe(1)–Fe(2)–H	132	131	38	38
Fe(1)–C(1)–O(1)	123	124	113	113
H–Fe(2)–C(1)	162	162	–	–

Vibrational Spectroscopy

Raman and IR spectroscopy were performed on the two isomers and the corresponding deuterated complexes (*D*-term and μ-D) in order to identify the Fe–H stretch, ν(Fe–H). Identification of this mode for *H*-term and μ-H would allow an additional evaluation of the DFT results compared to experiment in addition to the structural comparisons. Initial results from resonance Raman display very low signal intensity (not shown) in contrast to the results for [(μ-edt)$Fe_2(CO)_6$] studied before,[69] which prompted us to study the complexes with non-resonance Raman spectroscopy by using excitation wavelengths of 785 and 1064 nm. Figures 3 and 4 show the Raman spectra of the μ-H and μ-D complexes, respectively. The room temperature spectra show distinct signals at 1928 and 1934 cm^{-1}, which correspond to the two terminal ν(C=O) stretching modes, $\nu(C=O)_{term}$. The calculated ν(C=O) frequencies for this isomer are 1939 and 1943 cm^{-1}, which correspond to the antisymmetric and symmetric C=O stretching vibrations, respectively. The calculated ν(C=O) frequencies are therefore in excellent agreement with the experimental data – overestimating the energies of these modes by only ca. 10 cm^{-1}. A peak at 1220 cm^{-1} is observed for μ-H, which shifts to 891/1009 cm^{-1} for μ-D. DFT calculations (BP86/TZVP, Supporting Information, Figure S1) predict two ν(Fe–H) stretching modes in μ-H at 1151 and 1352 cm^{-1}, which correspond to the antisymmetric and symmetric Fe–H–Fe stretches, respectively (Figure 5). Upon deuteration, the stretching modes are predicted to shift to 871 and 963 cm^{-1}, respectively. On the basis of the DFT results, the observed peak at 1220 cm^{-1} likely corresponds to the antisymmetric ν_{as}(Fe–H) stretch, predicted at 1151 cm^{-1}. The calculations therefore underestimate this mode by ca. 70 cm^{-1}, which is in reasonable agreement with the experimental value. The reason for the absence of the symmetric Fe–H stretch in the experimental data is unknown. In the lower-energy region (200–740 cm^{-1}), the spectra of μ-H and μ-D are similar, which suggests this region to be dominated by inner ligand vibrations of the coordinated phosphane and bridging thiolate ligands. Unlike the μ-H complex, the corresponding *H*-term isomer is unstable at room temperature and, hence, easily decomposes upon irradiation, as shown by imaging. Data were obtained on the *D*-term isomer (Supporting Information, Figure S2), where a ν(C=O) peak at 1931 cm^{-1} is observed (terminal CO group), $\nu(C=O)_{term}$, on the basis of a comparison with the IR spectrum of the complex (discussed next). The predicted (BP86/TZVP) ν(Fe–H) stretching mode for *H*-term is at 1908 cm^{-1} (Supporting Information, Figure S3).

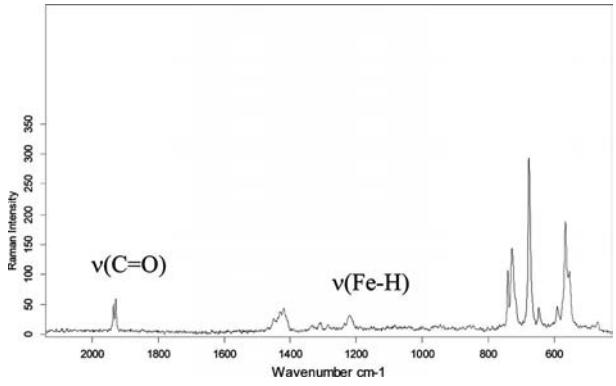

Figure 3. Raman spectra of solid μ-H (μ-edt)$[Fe_2(PMe_3)_4(CO)_2H]^+$ by using an excitation wavelength of 785 nm.

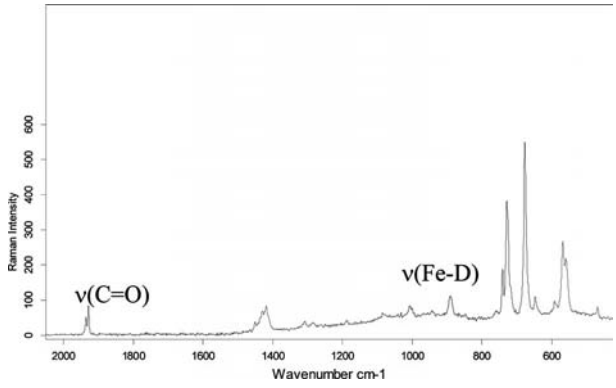

Figure 4. Raman spectra of solid μ-D (μ-edt)$[Fe_2(PMe_3)_4(CO)_2D]^+$ by using an excitation wavelength of 785 nm.

Because of the instability of the terminal hydride complex upon laser excitation, a less-destructive vibrational technique such as diffuse reflectance FT-IR spectroscopy was utilized. Figure 6 shows the solid-state IR spectra of *H*-term and μ-H. The spectra show distinct differences in the ν(C=O) region; however, the weak ν(Fe–H) stretching mode cannot be observed. The spectrum of *H*-term shows two distinct features at 1940 and 1840 cm^{-1} that correspond

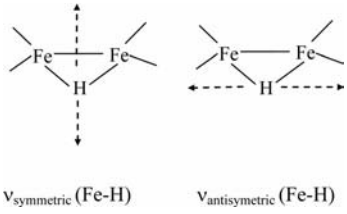

Figure 5. Schematic diagram of the symmetric and antisymmetric Fe–H stretches observed for μ-H.

to the terminal and bridging CO ligand stretches, respectively. Calculations predict these modes to occur at 1950 and 1860 cm^{-1} for the terminal and bridging ν(C=O) stretches, respectively, again showing that the DFT results adequately complement the experimental data. In acetonitrile solution, the band at 1840 cm^{-1} shifts to higher energy (1874 cm^{-1}), and a weak band at 1844 cm^{-1} is observed, which (according to the literature) is attributable to the ν(Fe–H) stretching mode.[66] However, this weak feature does not seem to be apparent in the solid-state IR spectra in comparison with the *D*-term IR data (Supporting Information, Figure S4). Hence, this assignment might not be correct. Unlike in *H*-term, the IR spectrum of μ-H shows one strong peak at 1928 cm^{-1}, which is consistent with the terminal ν(C=O) stretching vibrations. A weaker feature is observed at 1889 cm^{-1}, which is also present in the corresponding μ-D spectrum. The exact identity of this weak feature is unknown. In acetonitrile solution, the two terminal C–O stretching vibrations are observed at ca. 1940 and 1928 cm^{-1},[66] in accordance with the Raman data.

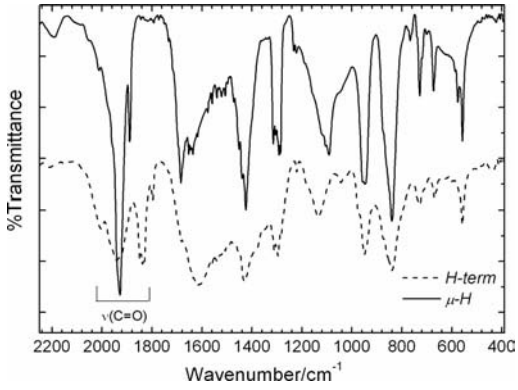

Figure 6. FT-IR spectra of solid *H*-term and μ-H isomers of (μ-edt)$[Fe_2(PMe_3)_4(CO)_2H]^+$.

Potential Energy Surface (PES) Calculations

Figure 7 shows the PES of the *H*-term and μ-H complexes upon addition of a proton source, nitropyridinium (B3LYP/TZVP). Potential proton sources such as H_3O^+, NH_4^+, pyridinium, and trifluoropyridinium were also tested but were either too strong or too weak. The choice of the acid is guided by the idea that the catalyst should be able to produce hydrogen by using weak acids, and this is the scenario that we are interested in investigating. The use of a strong acid such as HOTf or $H(OEt_2)_2BArF$ will provide a very strong thermodynamic driving force (i.e. the reaction is very exothermic), which thus reduces energy barriers that are relevant under conditions of weak acid strength. Acetic acid would be a good choice, but for computational reasons, a charge separation (i.e. $HA \rightarrow H^+ + A^-$) leads to significant problems in total energy calculations, as solvation of the generated ions becomes a very important part of the total energy. This effect cannot be described well computationally, in particular in a protic solvent. It is therefore advantageous to circumvent this problem by using a protonated amine or pyridine as acid (i.e. $HPy^+ \rightarrow H^+ +$ Py), where no additional ions are generated upon proton transfer. We therefore tried different pyridinium-based acids. Total energy calculations for *H*-term yield reaction energies for hydrogen generation of $\Delta E \approx +4$ kcal/mol for trifluoropyridinium and $\Delta E \approx +9$ kcal/mol for nitropyridinium. The latter weaker acid was then used for the PES calculations.

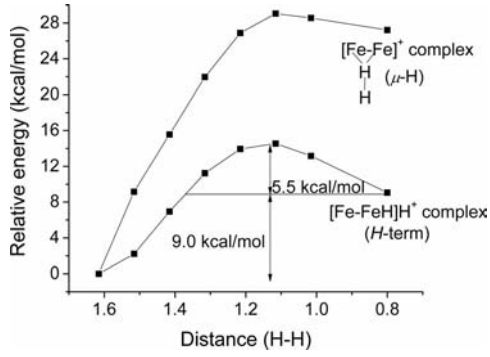

Figure 7. Potential energy surface (PES) plots for the reaction of the *H*-term and μ-H isomers of (μ-edt)$[Fe_2(PMe_3)_4(CO)_2H]^+$ with a proton source. B3LYP/TZVP was used to generate the PES plots. Energies are relative to the hydride complexes in Figure 2 (set to 0 kcal/mol in both cases).

As shown in Figure 7, the formation of the corresponding dihydrogen complexes for *H*-term and μ-H is endothermic in both cases. However, crucial differences are noticeable between the two PES plots, which may play an important role for the preferential protonation of *H*-term. In particular, the activation energy barrier for the formation of the *H*-term dihydrogen intermediate is 14.5 kcal/mol, which is exactly half the energy barrier observed for the μ-H hydride complex. The lower activation energy in the protonation of *H*-term is attributed to an increased stability of the formed H_2 intermediate in the *H*-term case. In addition, the energy barrier for the back reaction is 5.5 kcal/mol for *H*-term, whereas it is only 1.8 kcal/mol for μ-H. The dihydrogen complex of μ-H is therefore intrinsically unstable, and readily decomposes into the reactants before the base can dissociate. Protonation of *H*-term therefore has a greater kinetic driving force, favoring the formation of the corresponding dihydrogen complex. Interestingly, the DFT calculations predict that dihydrogen is bound end-on in the resulting complex, (μ-edt)$[Fe_2(PMe_3)_4(CO)_2H_2]^{2+}$. As shown in the Supporting Information Figure S5, the obtained Fe–H_2 distance is ca. 1.8 Å.

In summary, the greater reactivity of *H*-term towards the generation of hydrogen arises from both the lower activation energy for the protonation reaction and the stability of the dihydrogen complex formed. Although it has not been calculated for (μ-edt)$[Fe_2(PMe_3)_4(CO)_2H]^+$, it is interesting to note that in a computational study involving a $Ni^{II}Fe^{II}$ hydrogenase model complex, the effect of entropy on H_2 binding can be estimated to be ca. 10 kcal/mol.[70] By assuming the entropy to be similar for the protonation of *H*-term and μ-H, this entropic effect could provide the driving force for the release of H_2 after formation of the dihydrogen complex.

Figure 8 shows the H_2 complexes formed upon protonation of *H*-term and μ-H in the PES scans. Further calculations predict that *H*-term binds H_2 end-on, even in the absence of base, as mentioned above. In comparison, a [NiRu] complex modeling [NiFe] hydrogenase has been proposed (on the basis of DFT results) to coordinate H_2 in a side-on fashion.[71]

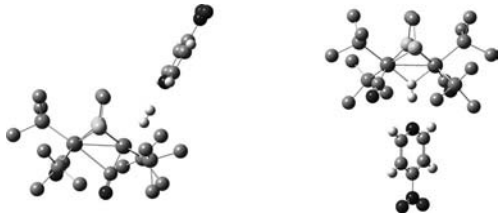

Figure 8. Dihydrogen complexes of the *H*-term (left) and μ-H (right) isomers of (μ-edt)$[Fe_2(PMe_3)_4(CO)_2H]^+$, obtained by using B3LYP/TZVP.

Single-Point Calculations

The atomic charge of hydride is a potential indicator of its propensity to accept a proton. Between the *H*-term and μ-H complex, it is expected that the former will exhibit a larger negative atomic charge on the basis that *H*-term is more reactive towards acid.[66] Surprisingly, the calculations show that the atomic charge of the *H*-term hydride is only slightly more negative than that of the hydride in the corresponding μ-H complex. This result implies that the total charge of the bound hydride does not contribute significantly to the difference in reactivity through charge control. Table 2 presents the atomic charges of the hydride for the *H*-term and μ-H (μ-edt)$[Fe_2(PMe_3)_4(CO)_2H]^+$ complexes.

Table 2. Calculated Fe–H hydride atomic charges in the *H*-term and μ-H isomers of (μ-edt)$[Fe_2(PMe_3)_4(CO)_2H]^+$.

Type of atomic charge	Fe–H atomic charges	
	H-term	μ-H
Löwdin	–0.0109	0.0783
Mulliken	–0.0426	0.0320

Another factor that potentially influences the reactivity of *H*-term towards acids is the nature of the frontier molecular orbitals (MOs). Figure 9 shows contour plots of important MOs for *H*-term. The highest occupied molecular orbital (HOMO) of *H*-term, MO <147>, has mostly Fe character showing 35% and 20% d_{xz} contributions from Fe(1) and Fe(2), respectively. The lowest unoccupied molecular orbital (LUMO), MO <148>, has some Fe character [24% d_{z^2} from Fe(1); 9% d_{z^2} from Fe(2)] and minor contributions from the terminal hydride [3% H(1s)]. Interestingly, *H*-term has a key MO (<139>) at a relatively high energy that shows a strong hydride (1s) contribution of 23%, as well as 24% Fe(2) d_σ character. This orbital therefore constitutes the Fe–H σ bond. The corresponding antibonding combination of this key orbital is MO <151>, which has 10% 1s hydride and 21% Fe(2) d_σ character.

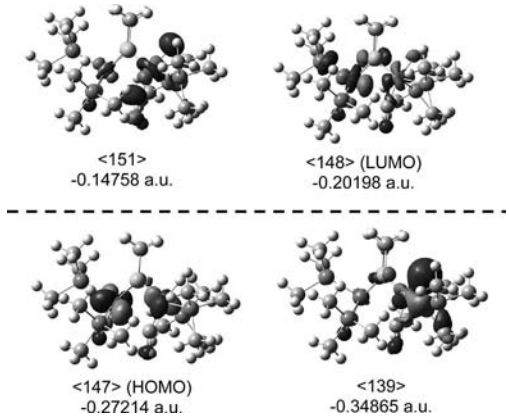

Figure 9. Contour plots of selected MOs of *H*-term (μ-edt)-$[Fe_2(PMe_3)_4(CO)_2H]^+$ calculated with BP86/TZVP.

The corresponding key MOs for the μ-H complex are presented in Figure 10. The HOMO, MO <147>, shows dominant metal character [36% and 31% d_{xz} from Fe(1) and Fe(2), respectively]. The corresponding LUMO, MO <148>, shows contributions from both iron centers [20% d_{z^2} for both Fe(1) and Fe(2)], as well as minor phosphane and sulfur character. The HOMO and LUMO of μ-H are therefore quite similar (but more symmetric) compared to *H*-term. The Fe–H bonding MOs in the case of μ-H are MO <138> [9% H(1s)] and <156> [12% H(1s)]. However, unlike the *H*-term complex that shows 23% hydride character in the Fe–H bonding MO (<139>), the μ-H counter-

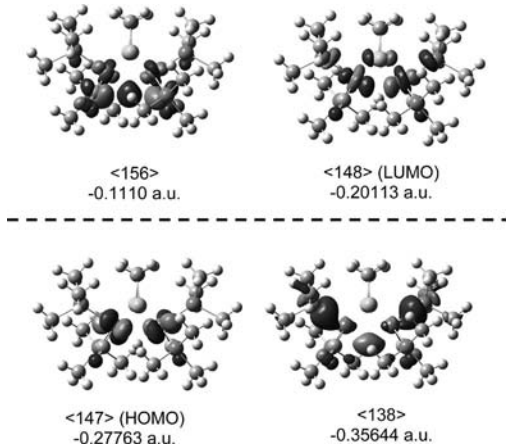

Figure 10. Contour plots of selected MOs of μ-H (μ-edt)$[Fe_2(PMe_3)_4(CO)_2H]^+$ calculated with BP86/TZVP.

part, MO <138>, has less hydride character and a lower energy. This key difference indicates a possible orbital (kinetic) control of the reaction of *H*-term with acid as a major contribution to the lower activation energy, and, hence, enhanced reactivity of *H*-term.

Summary and Conclusions

Solid-state IR and Raman measurements, and DFT calculations were performed on the *H*-term and μ-H isomers of (μ-edt)$[Fe_2(PMe_3)_4(CO)_2H]^+$. Comparison of structural and vibrational data between the DFT calculations and experiment show that the calculations reproduce the properties of both of these isomers well. In addition, the calculations allow us to further assign the vibrational spectra. The *ν*(Fe–H) vibrational mode was identified at 1220 cm^{-1} for μ-H through Raman spectroscopy, but remains elusive for the corresponding *H*-term complex because of its instability at room temperature. DFT calculations show that μ-H is 12.7 kcal/mol more stable than *H*-term, which may account for its decreased reactivity towards acid. This is comparable to a previous DFT study on the terminal and bridging hydride isomers of a [FeFe] hydrogenase active site model, which shows the latter isomer to be 10–12 kcal/mol more stable.[65] Importantly, our PES calculations show that the barrier for protonation of *H*-term is significantly lower than that of μ-H. We speculate that this lower energy barrier for *H*-term may relate to the presence of a frontier MO that has a high contribution of hydride 1s character in this case (orbital control of the reaction). The DFT calculations therefore strongly support the preferred protonation of the *H*-term complex over μ-H. Lastly, the resulting H_2 intermediate is stabilized in the *H*-term complex, but not μ-H. In summary, these combined findings explain why, experimentally, *H*-term reacts with acids to form H_2, whereas μ-H does not.

Despite the difference in energy barrier between the two hydride complexes, the barrier for protonation of *H*-term is still quite significant. From these observations, we conclude that the protonation of μ-H does not occur, while that of *H*-term should be relatively slow. *We propose that in order for fast turnover and H_2 generation to occur as observed in the enzyme, the H-term diferrous complex will have to be further activated to enable fast reaction with a proton source.* This could be achieved by one-electron reduction of the hydride complex prior to protonation and H_2 formation. In this way, the barrier for protonation could significantly be lowered, thus accelerating the overall reaction rate of the complexes with acids. Therefore, these results provide further evidence for a proton–electron–proton–electron transfer sequence in the mechanism of the enzyme [FeFe] hydrogenase.

Experimental Section

DFT Calculations: The geometries of the *H*-term and μ-H isomers of (μ-edt)$[Fe_2(PMe_3)_4(CO)_2H]^+$ were optimized in the gas phase by using the gradient-corrected functional BP86 and Ahlrich's triple-ξ valence polarization (TZVP) basis set as implemented in Gaussian 03.[72] Frequency calculations were performed on the optimized structures by using the same functional and basis set. The potential energy surface (PES) calculations employed B3LYP/TZVP geometry optimizations, where the H–H(–Fe) distances were fixed and all other internal coordinates were allowed to vary (Scheme 2). 4-Nitropyridinium was used as the proton source. In order to generate the molecular orbitals, single-point calculations (BP86/TZVP) were performed on the fully optimized structures of the two complexes by using the program ORCA.[73] Orbitals were plotted with GaussView v.3.0.

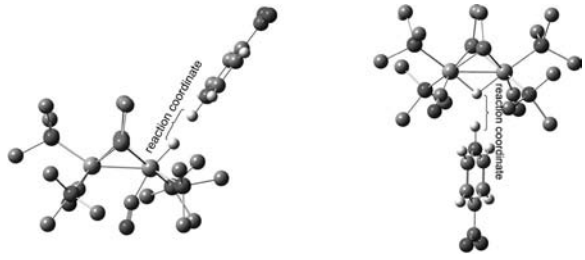

Scheme 2. Hydride complexes of the *H*-term (left) and μ-H (right) isomers of (μ-edt)$[Fe_2(PMe_3)_4(CO)_2H]^+$. The reaction coordinates used for the PES scans (B3LYP/TZVP) are shown by brackets.

Synthesis of (μ-edt)$[Fe_2(PMe_3)_4(CO)_2H]BF_4$: The terminal and bridging hydride isomers of (μ-edt)$[Fe_2(PMe_3)_4(CO)_2H]BF_4$ and the corresponding deuterated complexes were prepared as described previously.[66]

Raman and Infrared Spectroscopy: Raman data were obtained on solid samples of the model complexes (approximately 5 mg) on two different spectrometers. The first instrument, a Bruker Senterra Raman, employs 785-nm excitation and affords a spectral resolution of 3 cm^{-1}. The excitation beam from the laser (25 mW) was focused on the sample, and the scattered photons were detected by a CCD camera. The second system employs 1064 nm excitation light by using a Bruker Ram II FT-Raman module on a Vertex 70 FT-IR spectrometer. An excitation power of 100 mW was used, and the scattered photons were focused on a LN-Ge diode detector. The diffuse reflectance FT-IR spectra were recorded on a Perkin–Elmer Spectrum GX FT-IR at room temperature by using a powdered sample (approximately 5 mg) diluted with KBr.

Supporting Information (see footnote on the first page of this article): The DFT-predicted Raman spectra of the *H*-term and μ-H isomers of (μ-edt)$[Fe_2(PMe_3)_4(CO)_2H]^+$, the FT-Raman spectrum of solid *D*-term (μ-edt)$[Fe_2(PMe_3)_4(CO)_2D]^+$, the FT-IR spectra of *H*-term and *D*-term (μ-edt)$[Fe_2(PMe_3)_4(CO)_2$ H/D$]^+$, the calculated structure of the dihydrogen complex of *H*-term upon removal of nitropyridine, and colored versions of the geometry-optimized structures and MO contour plots are presented.

Acknowledgments

This work was supported by the ACS Petroleum Research Fund (PRF # 47013-G3) and the University of Michigan Office of the Vice President for Research (OVPR # 5805) (both to N. L.). C. M. W. is supported by the National Institutes of Health. We thank Prof. Thomas Rauchfuss (UIUC) for helpful discussions.

[1] J. W. Peters, W. N. Lanzilotta, B. J. Lemon, L. C. Seefeldt, *Science* **1998**, *282*, 1853–1858.

[2] Y. Nicolet, C. Piras, P. Legrand, C. E. Hatchikian, J. C. Fontecilla-Camps, *Struct. Fold. Des.* **1999**, *7*, 13–23.
[3] A. Volbeda, M.-H. Charon, C. Piras, E. C. Hatchikian, M. Frey, J. C. Fontecilla-Camps, *Nature* **1995**, *373*, 580–587.
[4] A. Volbeda, E. Garcin, C. Piras, A. L. d. Lacey, V. M. Fernandez, E. C. Hatchikian, M. Frey, J. C. Fontecilla-Camps, *J. Am. Chem. Soc.* **1996**, *118*, 12989–12996.
[5] R. K. Thauer, A. R. Klein, G. C. Hartmann, *Chem. Rev.* **1996**, *96*, 3031–3042.
[6] C. Zirngibl, R. Hedderich, R. K. Thauer, *FEBS Lett.* **1990**, *261*, 112–116.
[7] E. C. Hatchikian, N. Forget, V. M. Fernandez, R. Williams, R. Cammack, *Eur. J. Biochem.* **1992**, *209*, 357–365.
[8] M. W. W. Adams, *Biochim. Biophys. Acta Bioenerg.* **1990**, *1020*, 115–145.
[9] A. L. D. Lacey, C. Stadler, C. Cavazza, E. C. Hatchikian, V. M. Fernandez, *J. Am. Chem. Soc.* **2000**, *122*, 11232–11233.
[10] A. J. Pierik, M. Hulstein, W. R. Hagen, S. P. Albracht, *Eur. J. Biochem.* **1998**, *258*, 572–578.
[11] Y. Nicolet, A. d. Lacey, X. Vernede, V. M. Fernandez, E. C. Hatchikian, J. C. Fontecilla-Camps, *J. Am. Chem. Soc.* **2001**, *123*, 1596–1601.
[12] G. Silakov, B. Wenk, E. Reijerse, W. Lubitz, *Phys. Chem. Chem. Phys.* **2009**, *11*, 6592–6599.
[13] U. Ryde, C. Greco, L. De Gioia, *J. Am. Chem. Soc.* **2010**, *132*, 4512–4513.
[14] X. Zhao, I. P. Georgakaki, M. L. Miller, J. C. Yarbrough, M. Y. Darensbourg, *J. Am. Chem. Soc.* **2001**, *123*, 9710–9711.
[15] S. Ott, M. Kritikos, B. Åkermark, L. Sun, R. Lomoth, *Angew. Chem.* **2004**, *116*, 1024; *Angew. Chem. Int. Ed.* **2004**, *43*, 1006–1009.
[16] L. Schwartz, G. Eilers, L. Eriksson, A. Gogoll, R. Lomoth, S. Ott, *Chem. Commun.* **2006**, 520–522.
[17] C. Tard, X. Liu, K. Ibrahim Saad, M. Bruschi, L. De Gioia, S. C. Davies, X. Yang, L.-S. Wang, G. Sawers, C. J. Pickett, *Nature* **2005**, *433*, 610–613.
[18] M. Schmidt, S. M. Contakes, T. B. Rauchfuss, *J. Am. Chem. Soc.* **1999**, *121*, 9736–9737.
[19] E. J. Lyon, I. P. Georgakaki, J. H. Reibenspies, M. Y. Darensbourg, *Angew. Chem.* **1999**, *111*, 3373; *Angew. Chem. Int. Ed.* **1999**, *38*, 3178–3180.
[20] A. Le Cloirec, S. P. Best, S. Borg, S. C. Davies, D. H. Evans, D. L. Hughes, C. J. Pickett, *Chem. Commun.* **1999**, 2285–2286.
[21] F. Gloaguen, J. D. Lawrence, M. Schmidt, S. R. Wilson, T. B. Rauchfuss, *J. Am. Chem. Soc.* **2001**, *123*, 12518–125727.
[22] J. L. Nehring, D. M. Heinekey, *Inorg. Chem.* **2003**, *42*, 4288–4292.
[23] I. P. Georgakaki, M. L. Miller, M. Y. Darensbourg, *Inorg. Chem.* **2003**, *42*, 2489–2494.
[24] S. Ott, M. Kritikos, B. Akermark, L. Sun, *Angew. Chem.* **2003**, *115*, 3407; *Angew. Chem. Int. Ed.* **2003**, *42*, 3285–3288.
[25] J. W. Tye, J. Lee, H.-W. Wang, R. Mejia-Rodriguez, J. H. Reibenspies, M. B. Hall, M. Y. Darensbourg, *Inorg. Chem.* **2005**, *44*, 5550–5552.
[26] C. A. Boyke, J. I. van der Vlugt, T. B. Rauchfuss, S. R. Wilson, G. Zampella, L. De Gioia, *J. Am. Chem. Soc.* **2005**, *127*, 11010–11018.
[27] W. Dong, M. Wang, X. Liu, K. Jin, G. Li, F. Wang, L. Sun, *Chem. Commun.* **2006**, 305–307.
[28] D. Morvan, J.-F. Capon, F. Gloaguen, A. Le Goff, M. Marchivie, F. Michaud, P. Schollhammer, J. Talarmin, J.-J. Yaouanc, *Organometallics* **2007**, *26*, 2042–2052.
[29] S. Jiang, J. Liu, Y. Shi, Z. Wang, B. Åkermark, L. Sun, *Dalton Trans.* **2007**, 896–902.
[30] D. Morvan, J.-F. Capon, F. Gloaguen, P. Schollhammer, J. Talarmin, *Eur. J. Inorg. Chem.* **2007**, *32*, 5062–5068.
[31] S. Ezzaher, J.-F. Capon, F. Gloaguen, F. Y. Petillon, P. Schollhammer, J. Talarmin, *Inorg. Chem.* **2007**, *46*, 9863–9872.
[32] F. Wang, M. Wang, X. Liu, K. Jin, W. Dong, L. Sun, *Dalton Trans.* **2007**, *34*, 3812–3819.
[33] G. Eilers, L. Schwartz, M. Stein, G. Zampella, L. De Gioia, S. Ott, R. Lomoth, *Chem. Eur. J.* **2007**, *13*, 7075–7084.
[34] A. K. Justice, G. Zampella, L. De Gioia, T. B. Rauchfuss, *Chem. Commun.* **2007**, 2019–2021.
[35] Z. Yu, M. Wang, P. Li, W. Dong, F. Wang, L. Sun, *Dalton Trans.* **2008**, *18*, 2400–2406.
[36] L.-C. Song, L.-X. Wang, B.-S. Yin, Y.-L. Li, X.-G. Zhang, Y.-W. Zhang, X. Luo, Q.-M. Hu, *Eur. J. Inorg. Chem.* **2008**, 291–297.
[37] N. Wang, M. Wang, T. Zhang, P. Li, J. Liu, L. Sun, *Chem. Commun.* **2008**, *44*, 5800–5802.
[38] C. M. Thomas, T. Liu, M. B. Hall, M. Y. Darensbourg, *Inorg. Chem.* **2008**, *47*, 7009–7024.
[39] A. K. Justice, L. De Gioia, M. J. Nilges, T. B. Rauchfuss, S. R. Wilson, G. Zampella, *Inorg. Chem.* **2008**, *47*, 7405–7414.
[40] P. Li, M. Wang, L. Chen, J. Liu, Z. Zhao, L. Sun, *Dalton Trans.* **2009**, 1919–1926.
[41] X. de Hatten, E. Bothe, K. Merz, I. Huc, N. Metzler-Nolte, *Eur. J. Inorg. Chem.* **2008**, 4530–4537.
[42] S. Ezzaher, J.-F. Capon, F. Gloaguen, F. Y. Petillon, P. Schollhammer, J. Talarmin, *Inorg. Chem.* **2009**, *48*, 2–4.
[43] L.-C. Song, L.-X. Wang, M.-Y. Tang, C.-G. Li, H.-B. Song, Q.-M. Hu, *Organometallics* **2009**, *28*, 3834–3841.
[44] F. I. Adam, G. Hogarth, I. Richards, B. E. Sanchez, *Dalton Trans.* **2007**, 2495–2498.
[45] W. Gao, J. Ekstrom, J. Liu, C. Chen, L. Eriksson, L. Weng, B. Akermark, L. Sun, *Inorg. Chem.* **2007**, *46*, 1981–1991.
[46] L. Duan, M. Wang, P. Li, Y. Na, N. Wang, L. Sun, *Dalton Trans.* **2007**, 1277–1283.
[47] P.-Y. Orain, J.-F. Capon, N. Kervarec, F. Gloaguen, F. Y. Petillon, R. Pichon, P. Schollhammer, J. Talarmin, *Dalton Trans.* **2007**, 3754–3756.
[48] A. K. Justice, G. Zampella, L. De Gioia, T. B. Rauchfuss, J. I. van der Vlugt, S. R. Wilson, *Inorg. Chem.* **2007**, *46*, 1655–1664.
[49] N. Wang, M. Wang, T. Liu, P. Li, T. Zhang, M. Y. Darensbourg, L. Sun, *Inorg. Chem.* **2008**, *47*, 6948–6955.
[50] J.-F. Capon, S. Ezzaher, F. Gloaguen, F. Y. Petillon, P. Schollhammer, J. Talarmin, *Chem. Eur. J.* **2008**, *14*, 1954–1964.
[51] A. T. Fiedler, T. C. Brunold, *Inorg. Chem.* **2005**, *44*, 1794–1809.
[52] M. Y. Darensbourg, E. J. Lyon, X. Zhao, I. P. Georgakaki, *Proc. Natl. Acad. Sci. USA* **2003**, *100*, 3683–3688.
[53] T. Zhou, Y. Mo, A. Liu, Z. Zhou, K. R. Tsai, *Inorg. Chem.* **2004**, *43*, 923–930.
[54] X. Zhao, I. P. Georgakaki, M. L. Miller, R. Mejia-Rodriguez, C. Y. Chiang, M. Y. Darensbourg, *Inorg. Chem.* **2002**, *41*, 3917.
[55] S. J. Borg, T. Behrsing, S. P. Best, M. Razavet, X. Liu, C. J. Pickett, *J. Am. Chem. Soc.* **2004**, *126*, 16988–16999.
[56] S. D. Brown, M. P. Mehn, J. C. Peters, *J. Am. Chem. Soc.* **2005**, *127*, 13146.
[57] M. Bruschi, P. Fantucci, L. De Gioia, *Inorg. Chem.* **2002**, *41*, 1421.
[58] J. Zhou, Y. R. Mo, Z. H. Zhou, K. Tsal, *Inorg. Chem.* **2005**, *44*, 4941.
[59] J. A. Wright, C. J. Pickett, *Chem. Commun.* **2009**, 5719–5721.
[60] A. Jablonskytė, J. A. Wright, C. J. Pickett, *Dalton Trans.* **2010**, *39*, 3026–3034.
[61] Y. Nicolet, B. J. Lemon, J. C. Fontecilla-Camps, J. W. Peters, *Trends Biochem. Sci.* **2000**, *25*, 138.
[62] Z. Cao, M. B. Hall, *J. Am. Chem. Soc.* **2001**, *123*, 3734–3742.
[63] B. J. Lemon, J. W. Peters, *J. Am. Chem. Soc.* **2000**, *122*, 3793.
[64] Z. Liu, P. Hu, *J. Chem. Phys.* **2002**, *117*, 8177.
[65] G. Zampella, C. Greco, P. Fantucci, L. De Gioia, *Inorg. Chem.* **2006**, *45*, 4109–4118.
[66] J. I. van der Vlugt, T. B. Rauchfuss, C. M. Whaley, S. R. Wilson, *J. Am. Chem. Soc.* **2005**, *127*, 16012–16013.
[67] L. D. Betowski, M. Enlow, *THEOCHEM* **2003**, *638*, 189–195.
[68] A. Schafer, H. Horn, R. Ahlrichs, *J. Phys. Chem.* **1992**, *97*, 2571–2577.
[69] M. G. I. Galinato, C. M. Whaley, N. Lehnert, *Inorg. Chem.* **2010**, *49*, 3201–3215.

[70] P. E. M. Siegbahn, J. W. Tye, M. B. Hall, *Chem. Rev.* **2007**, *107*, 4414–4435.
[71] L. Vaccaro, V. Artero, S. Canaguier, M. Fontecave, M. J. Field, *Dalton Trans.* **2010**, *39*, 3043–3049.
[72] M. J. Frisch, G. W. Trucks, H. B. Schlegel, G. E. Scuseria, M. A. Robb, J. R. Cheeseman, J. A. M. T. Vreven Jr., K. N. Kudin, J. C. Burant, J. M. Milliam, S. S. Lyengar, J. Tomasi, V. Barone, B. Mennucci, M. Cossi, G. Scalmani, N. Rega, G. A. Petersson, H. Nakatsuji, M. Hada, M. Ehara, K. Toyota, R. Fukuda, J. Hasegawa, M. Ishida, T. Nakajima, Y. Honda, O. kitao, H. Nakai, M. Klene, X. Li, J. E. Knox, H. P. Hratchian, J. B. Cross, V. Bakken, C. Adamo, J. Jaramillo, R. Gomperts, R. E. Stratmann, O. Yazyev, A. J. Austin, R. Cammi, C. Pomelli, J. W. Ochterski, P. Y. Ayala, K. Morokuma, G. A. Voth, P. Salvador, J. J. Danneberg, V. G. Zakrewski, S. Dapprich, A. D. Daniels, M. C. Strain, O. Farkas, D. K. Malick, A. D. Rabuck, K. Raghavachari, J. B. Foresman, J. V. Ortiz, Q. Cui, A. G. Baboul, S. Clifford, J. Cioslowski, B. B. Stefanov, G. Liu, A. Liashenko, P. Piskorz, I. Komaromi, R. L. Martin, D. J. Fox, T. Keith, M. A. Al-Laham, C. Y. Peng, A. Nanayakkara, M. Challacombe, P. M. W. Gill, B. Johnson, W. Chen, M. W. Wong, C. Gonzalez, J. A. Pople, *Gaussian 03*, Gaussian, Inc., Pittsburgh, PA, **2003**.
[73] F. Neese, *ORCA version 2.6*, Institut für Physikalische und Theoretische Chemie, Universität Bonn, Bonn, Germany, **2007**.

Received: September 29, 2010
Published Online: January 20, 2011

